In memory of Professor Robert R. Gałązka

Magnetic Exchange Constant and Ferroelectric Anomaly in Magnetic Susceptibility in $Sn_{1-x-y}Si_xMn_yTe$ Diluted Magnetic Semiconductors

L. Kilanski[a,*], M. Arciszewska[a], A. Khaliq[a], B. Brodowska[a], R. Minikayev[a] and V.E. Slynko[b]

[a] *Institute of Physics, Polish Academy of Sciences, Aleja Lotnikow 32/46, PL-02668 Warsaw, Poland*
[b] *Institute of Materials Science Problems, Ukrainian Academy of Sciences, 5 Wilde Str., 58001 Chernivtsi, Ukraine*

Doi: 10.12693/APhysPolA.141.161 *e-mail: kilan@ifpan.edu.pl

We present the studies of magnetic and electrical properties of $Sn_{1-x-y}Si_xMn_yTe$ mixed crystals. The magnetic susceptibility measurements revealed the presence of two types of transitions interpreted as a paramagnet–ferromagnet transition at $T < 10$ K due to carrier mediated Ruderman–Kittel–Kasuya–Yosida magnetic interactions and the anomaly related to the structural transition to the rhombohedral phase at $T \approx 75$ K. The presence of a well-defined magnetic hysteresis with a square shape confirms that the ferromagnetic state present in our samples is related to the homogeneous magnetic domain structure with narrow domain energy distribution. The contents of the magnetic ions determined via magnetometric methods is lower than the Mn contents determined via the energy dispersive X-ray fluorescence spectroscopy method indicating the presence of a large fraction of Mn ions being either short range coupled into small clusters like pairs, triples, or other entities or having lower total magnetic momentum than Mn in high-spin state. The magnetic exchange constant of our samples is equal to 0.25–0.3 eV indicating an increase with respect to ternary $Sn_{1-x}Mn_xTe$.

topics: transition-metal compounds, magnetic semiconductors

1. Introduction

IV–VI diluted magnetic semiconductors (DMSs) offer unique possibilities for simultaneous and independent control of electrical and magnetic properties of the system. It has been proven that the ferromagnetism in IV–VI DMSs is due to carrier mediated long range Ruderman–Kittel–Kasuya–Yosida (RKKY) magnetic interactions [1, 2] making them the ideal candidates for being used in semiconductor spintronic devices [3]. Group IV–VI semimagnetic semiconductors have an advantage over canonical materials of groups II–VI and III–V due to the possibility of simultaneous and independent control of electrical and magnetic properties [4]. In the past, several different papers were devoted to ternary DMSs showing the presence of either ferromagnetic or spin-glass order at $T < 20$ K [5–9]. The magnetic exchange constant related to the RKKY mechanism of indirect magnetic exchange J_{pd}, has rather low values for $Sn_{1-x}Mn_xTe$, not exceeding 0.1 eV for $x \leq 0.1$ [10].

In this manuscript, we present the studies of electrical and magnetic properties of $Sn_{1-x-y}Si_xMn_yTe$ DMS's with different chemical composition. The main goal of this work is to show the influence of considerable Si-alloying on the magnetic and electrical properties of the system. In particular, we wish to study whether the magnetic exchange coupling constant was influenced by the addition of silicon ions to the alloy. The value of J_{pd} should be inversely proportional to the cation mass, so the addition of Si should lead to a slight increase in J_{pd} value. This hypothesis needs to be verified within the scope of this manuscript. The second goal of this work is to show the appearance of an anomaly in the magnetic susceptibility at around 78 K. The physical mechanisms of this anomaly are discussed.

2. Sample preparation

The $Sn_{1-x-y}Si_xMn_yTe$ ingot (with total $x = 0.03$ and $y = 0.05$) was grown from a mixture of chemically pure components by the modified vertical Bridgman method. The essence of the modification consisted in creating a stationary transverse temperature gradient in the melt, which improved the mixing of the melt near the crystallization front and, accordingly, the homogeneity of the grown ingot.

TABLE I

Results of the characterization of the $Sn_{1-x-y}Si_xMn_yTe$ samples with different chemical compositions, x and y, including magnetotransport data obtained at $T = 4.3$ K, the carrier concentration n, the carrier mobility μ, and the magnetic properties: the Curie temperature T_C, the anomaly temperature T_F, the Curie–Weiss temperature θ, the Curie constant C, the effective Mn content y_θ determined from (2), the saturation magnetization M_s, determined using (3), and the effective Mn content y_m, determined using (4).

x ($\times 10^{-2}$)	y ($\times 10^{-2}$)	a [Å]	n ($\times 10^{20}$) [cm^{-3}]	μ [cm^2/(V s)]	T_C [K]	T_F [K]	θ [K]	C ($\times 10^{-4}$) [emu K/g]	y_θ ($\times 10^{-2}$)	M_s [emu/g]	y_m ($\times 10^{-2}$)
2.9 ± 0.3	4.1 ± 0.4	6.3142 ± 0.0002	8.8 ± 0.5	63 ± 3	5.0 ± 0.1	74.4 ± 0.7	20.0 ± 0.2	5.2 ± 0.2	1.3 ± 0.1	4.4 ± 0.1	2.2 ± 1
3.1 ± 0.3	4.6 ± 0.4	6.3051 ± 0.0002	8.4 ± 0.4	62 ± 2	6.2 ± 0.1	74.5 ± 0.5	22.5 ± 0.1	6.1 ± 0.4	1.5 ± 0.2	4.9 ± 0.1	2.5 ± 1
3.5 ± 0.4	4.9 ± 0.5	6.3064 ± 0.0002	7.3 ± 0.8	62 ± 4	7.2 ± 0.2	75.1 ± 0.4	23.4 ± 0.2	6.9 ± 0.3	1.7 ± 0.2	5.5 ± 0.1	2.8 ± 1
3.1 ± 0.3	5.1 ± 0.5	6.3116 ± 0.0002	6.3 ± 0.7	61 ± 3	8.4 ± 0.1	75.3 ± 0.4	24.0 ± 0.1	7.3 ± 0.2	1.8 ± 0.1	6.0 ± 0.1	3.0 ± 1

The components were weighed with an accuracy of ± 0.05 mg with a total ingot weight of 30 g. The inner surface of the quartz growth ampoule was covered with a strong graphite film ($T_m = 3826$°C [11]) to avoid direct contact of the quartz with the melt ($T_m = 1470$–1726°C [11]) and prevent the cooled ingot from sticking to the ampoule walls.

The growth ampoule with the charge was evacuated to 10^{-5} Torr, after which it was placed in the growth furnace and heated to 1300°C, which approximately corresponds to the temperature of the onset of quartz softening. For reliability, the growth ampoule with the charge was placed inside an external evacuated quartz ampoule, which was attached to the pulling mechanism. The rate of vertical drawing of the growth ampoule during directional crystallization was 1.5 mm/h with longitudinal temperature gradient at the crystallization front of 35°C/cm. Temperature stabilization and control in the growth furnace were carried out with accuracy of ± 0.01°C.

After the completion of crystal growth, the ingot was gradually cooled over 24 h to room temperature and removed from the growth furnace. The protective and growth quartz ampoules were partially flattened by atmospheric pressure due to deliberate overheating for the best dissolution of silicon and manganese in the SnTe crystal matrix. The finished ingot had an elliptical cross-section with major and minor axes from 13 to 16.3 mm and from 3.2 to 10.7 mm, respectively. The ingot was cut by an automated string into plates of the same thickness of 1.4 mm using Al_2O_3 abrasive, the maximum grain size of which did not exceed 40 μm.

3. Structural characterization

The structural characterization of the $Sn_{1-x-y}Si_xMn_yTe$ DMS's consisted of three measurement techniques: (i) energy dispersive X-ray fluorescence spectroscopy (EDXRF), (ii) high resolution X-ray diffraction (HRXRD) and (iii) scanning electron microscope (SEM) coupled with X-ray energy dispersive spectrometer (EDS) microprobe. Prior to the structural characterization, the as-grown ingots were cut into slices perpendicular to the growth direction. The growth specifics permit only small changes in the chemical composition of the crystals in the direction parallel to the growth direction. Therefore, we cut the as-grown slices using a wire saw into 1.5 mm thick slices in the direction perpendicular to the growth direction. This minimizes variations of the chemical composition within each individual slice. After cutting, the ingot slices were chemically cleaned using few organic solvents.

The EDXRF method was used to study the chemical compositions in the form of the distribution of alloying elements and determination of crystal stoichiometry as a function of the ingot length. The EDXRF measurements were made on both sides of each crystal slice. The obtained EDXRF spectra showed the correct stoichiometry for the majority of the crystal length. Only the initial and final smelting fragments did not maintain the correct stoichiometry and were therefore rejected from further studies. From all the slices, we selected a few in which the relative difference of the chemical composition was the smallest in the entire series.

The high-resolution X-ray diffraction (HRXRD) technique was used to determine the crystals' structure and phase composition of the studied samples. The HRXRD measurements were made using the X'Pert MPD Pro Alpha1, Panalytical diffractometer (Cu K_{α_1} with $\lambda = 1.540598$ Å). The obtained diffraction patterns for all our crystals were fitted with the use of the Rietveld method. The fits were possible for cubic NaCl structure only, indicating that our samples were single phased crystals. The lattice parameter values obtained during the Rietveld refinements (gathered in Table I) are close to the parameters known in the literature for SnTe with $a = 6.318(3)$ Å [12]. It is also evident that we observed a small decrease of the lattice parameter as a function of the sum of alloying elements. It is a signature of the successful growth of IV–VI DMS system.

4. Electrical characterization

The $Sn_{1-x-y}Si_xMn_yTe$ electrical properties were studied by means of temperature and magnetic field dependence conductivity and the Hall effect

measurements. Measurements were done with the use of iron-yoke magnet with a maximum $B < 1.5$ T and Oxford Instruments helium flow cryostat allowing precise temperature control in the range of $3 < T < 300$ K. All our magnetotransport measurements were made using standard six-contact Hall effect DC current technique. Electrical contacts to the sample were made using gold wire and indium solder.

Selected magnetotransport characterization values for our samples obtained at $T = 4.3$ K are gathered in Table I. All our samples show features typical of degenerate IV–VI semiconductors, the metallic shape of the temperature-dependent resistivity and strong p-type conductivity with high carrier concentration $n > 10^{20}$ cm^{-3} and moderate carrier mobility values $\mu < 70$ cm^2/(V s). While the carrier concentration for our samples has a value similar to that for SnTe [13], it seems that, in similarity to $Sn_{1-x}Mn_xTe$ [8], both Si- and Mn-alloying leads to lowering the carrier mobility, probably due to large concentrations of defects present in our samples.

5. Magnetometric results

The magnetic properties of the $Sn_{1-x-y}Si_xMn_yTe$ DMS's were studied with the use of the LakeShore 7229 susceptometer/magnetometer system. Two types of measurements were applied to the above-mentioned instrument: (i) dynamic magnetic susceptibility measured using mutual inductance method at controlled temperature T, varying in the range $1.4 < T < 320$ K, with the sample placed in the presence of the small AC magnetic field with frequency f, ranging from 7 to 9980 Hz, and amplitude H_{AC}, ranging up to 10 Oe, and (ii) static magnetization measurements using the Weiss extraction technique with the sample placed in the presence of magnetic field $B \leq 90$ kGs.

At first, we made a series of temperature dependent AC magnetic susceptibility measurements for all 4 samples selected for the present work. As a result of the AC susceptibility measurement the complex magnetic susceptibility values χ_{AC} were obtained, allowing decomposition into real and imaginary parts. The obtained results presented for the temperature dependence of the real part of the AC magnetic susceptibility are shown in Fig. 1.

Inspection of Fig. 1 shows clearly the presence of two maxima in $\mathrm{Re}(\chi_{AC})$ vs T dependences for all our samples. Rapid increase of $\mathrm{Re}(\chi_{AC})$ with lowering T, located at $T < 10$ K, is most probably the paramagnet-ferromagnet transition due to RKKY interactions in the system. The second increase of the $\mathrm{Re}(\chi_{AC})$ vs T dependence is observed for all our samples at $73 < T < 80$ K. At first glance, it looks like an anomaly in the magnetic susceptibility observed in SnTe is due to the paraelectric-ferroelectric transition associated with cubic–rhombohedral structural transition in

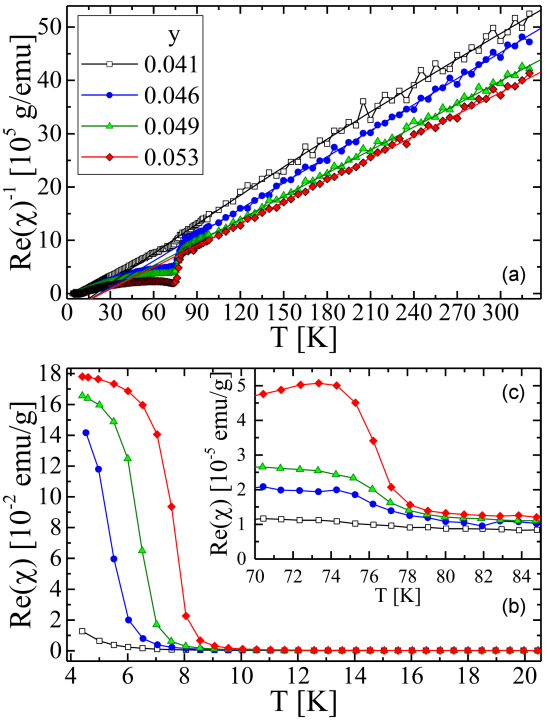

Fig. 1. Results of the AC magnetic susceptibility studies including the temperature dependence of (a) the inverse of the real part of the AC magnetic susceptibility and (b, c) the real part of the magnetic susceptibility with different chemical contents, i.e., x and y (labels).

SnTe-related alloys at low temperatures. Both the above speculations need to be verified by further data analysis and comparison with other data.

As a second step we performed a series of magnetization measurements, such as a function of the applied magnetic field, measured for each studied sample at several stabilized temperatures. The exemplary results of the magnetization measurements are presented in Fig. 2.

The magnetization of all our samples shows ferromagnetic Brillouin-like behavior with well-pronounced magnetic hysteresis at temperatures lower than the magnetic transition temperature. At temperatures higher than 8 K, our samples show a lack of magnetic hysteresis. It is therefore highly probable that the anomaly in the $\mathrm{Re}(\chi_{AC})$ vs T dependences observed at $T \approx 75$ K is not related to the magnetic order of Mn ions.

6. Data analysis and discussion

The magnetic interactions in Mn-alloyed SnTe crystals have been studied extensively in the past and revealed the presence of a magnetically ordered state in the system at temperatures lower than 20 K. It is therefore highly probable that the magnetic order observed in our samples has the same origin.

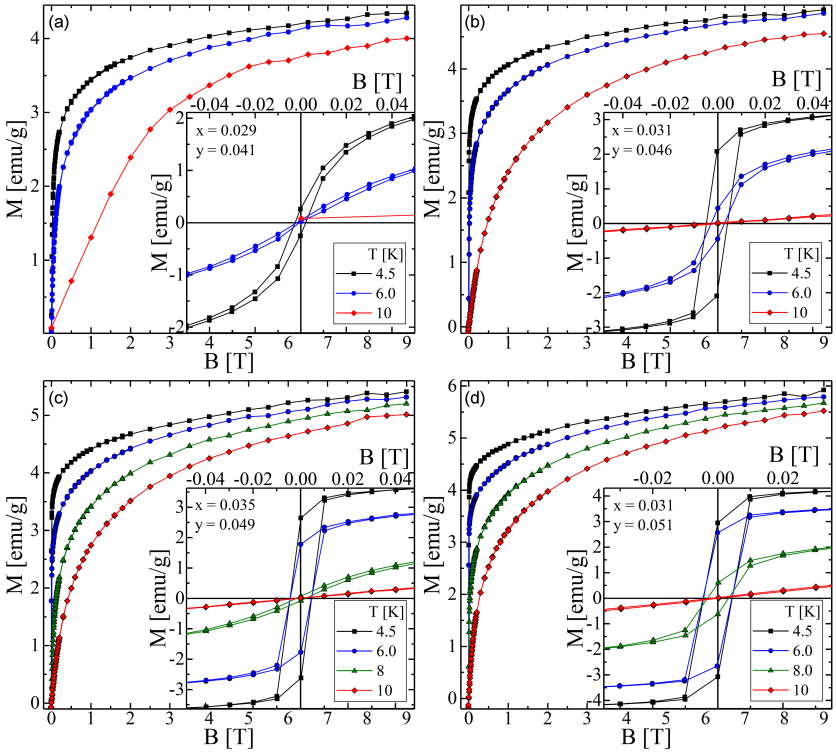

Fig. 2. Magnetization as a function of the magnetic field obtained at different temperatures for the studied $Sn_{1-x-y}Si_xMn_yTe$ samples with different chemical contents.

The temperature dependence of the inverse of the real part of the AC magnetic susceptibility, $[\mathrm{Re}(\chi_{\mathrm{AC}})]^{-1}$ vs T, serves as a valuable tool for determining the major exchange mechanism present in the material. The $[\mathrm{Re}(\chi_{\mathrm{AC}})]^{-1}$ vs T dependence for all our samples is presented in Fig. 1a. The obtained curves show the presence of two transitions: first at $T < 10$ K and a second one at $70 < T < 80$ K. At $T > 90$ K, however, the $[\mathrm{Re}(\chi_{\mathrm{AC}})]^{-1}$ vs T dependences for all our samples show linear behavior with increasing temperature up to 320 K, the maximum temperature of the experimental setup we used. Linear behavior of the $[\mathrm{Re}(\chi_{\mathrm{AC}})]^{-1}$ vs T dependence is a signature of the Curie–Weiss (C–W) law fulfilment in our samples. The modified C–W law for a system consisting of a diamagnetic lattice with paramagnetic ions can be expressed in the following form

$$\mathrm{Re}(\chi_{\mathrm{AC}}) = \frac{C}{T-\theta} + \chi_{\mathrm{dia}}, \tag{1}$$

where χ_{dia} is the diamagnetic contribution to the magnetic susceptibility originating from the SnTe lattice and C is the Curie constant given by the following equation

$$C = \frac{N_0 g^2 \mu_{\mathrm{B}}^2}{3k_{\mathrm{B}}} J(J+1)\, y_\theta, \tag{2}$$

where N_0 is the number of cations per gram, g is the effective g-factor of electrons in our samples, μ_{B} is the Bohr magneton, k_{B} is the Boltzmann constant, J is the total magnetic momentum of the Mn ions, and y_θ is the effective Mn content. The $[\mathrm{Re}(\chi_{\mathrm{AC}})]^{-1}$ vs T dependence for $T > 90$ K gathered in Fig. 1a is linear allowing us to fit this part of the $[\mathrm{Re}(\chi_{\mathrm{AC}})]^{-1}$ vs T dependence with the modified C–W law given with (1). Fitting procedure was done for $T > 120$ K with three fitting parameters: C, θ, and χ_{dia}. The results of the fitting procedure are presented as lines in Fig. 1a and the obtained fitting parameter values are gathered in Table I.

The obtained θ values for all our samples have positive values, slightly increasing as a function of the Mn content y. The positive θ sign is an important piece of information about the sign of the magnetic exchange constant in the material. It seems reasonable to say that the positive θ values are a signature of a ferromagnetic type of magnetic interaction dominating in our samples. During the modified C–W law fitting the χ_{dia}, values were determined. For all our samples we obtained negative $\chi_{\mathrm{dia}} \approx -2 \times 10^{-7}$ emu/g value, typical for IV–VI DMSs [14].

It seems reasonable to state that for our $Sn_{1-x-y}Si_xMn_yTe$ crystals, we observed paramagnet–ferromagnet transition. This statement is based on several facts: (i) the shape of the transition visible in Fig. 1b does not show any signatures of a cusp, (ii) we observed well-defined magnetic hysteresis at temperatures below the transition, and (iii) we obtained positive θ values. It allows us to determine the Curie temperature

T_C for all our samples by calculating the second derivative of the $\mathrm{Re}(\chi_{AC})$ vs T dependence and finding its inflection point. The T_C values obtained in the above way are presented in Table I. The T_C values are higher than the respective values for $Sn_{1-x}Mn_xTe$ [8], which may be an indication of an increase in the magnetic exchange constant in our samples with respect to $Sn_{1-x}Mn_xTe$ due to Si-alloying. This speculation will be verified later in this manuscript.

The Curie constant values gathered in Table I show an increase with increasing Mn content y. From the C values using (2), we can calculate the effective Mn-content y_θ. We assumed that the Mn^{2+} ions have spin-only magnetic moment $S = 5/2$, implying $J = S = 5/2$ in (2). Under this assumption, we obtained y_θ values for all our samples, gathered in Table I. It seems that for all our samples, $y_\theta < y$ and y/y_θ do not exceed 0.6 which is a common feature in IV–VI DMSs [14]. A part of this effect (a few percent) is related to the presence of Mn-pairs, -triples, and more complex short range positioning of Mn ions [15]. Such behavior is a natural consequence of a random distribution of Mn ions inside the semiconductor lattice. The rest of the Mn ions present in our samples may have a lower spin-state than $S = 5/2$ or be in a position where the orbital magnetic momentum is nonzero, thus reducing the total magnetic momentum per Mn ion.

Another interesting feature is observed in the $\mathrm{Re}(\chi_{AC})$ vs T dependence for all our samples at $T \approx 75$ K (see Fig. 1c). The presence of the second transition in magnetic susceptibility is seen in all our samples. The magnitude of the transition seems to be proportional to the Mn-content in the samples. It would be therefore natural to assume the presence of a second magnetic phase transition in these samples. This conclusion, however, is not supported by the magnetization results. All the $M(B)$ curves at $T > 10$ K show features typical of paramagnetic material. There seems to be no trace of this anomaly in the $M(B)$ curves at $T \approx 75$ K. It is therefore possible that this effect is not related to the Mn-ions but has a different origin. The presence of structural transition is visible in SnTe and $Sn_{1-x}Mn_xTe$ at about 80 K [16]. A similar anomaly was observed in thin $Sn_{1-x}Mn_xTe$ layers [8], but the Authors claimed that it is usually not observed in bulk crystals [8]. Therefore, we believe that our anomaly in $\mathrm{Re}(\chi_{AC})$ vs T dependence is related to the appearance of rhombohedral NaCl-structure distortion in our samples. The transition temperature of this anomaly seems to indicate that the rhombohedral distortion temperature is slightly lowered (by about 4–5 K) with respect to the SnTe and $Sn_{1-x}Mn_xTe$. We believe that it is due to the presence of Si ions.

The magnetization as a function of the magnetic field for our samples at $T < T_C$ shows features characteristic of a ferromagnet, a well-defined magnetic hysteresis with a square-like shape and coercive field slightly increasing as a function of the Mn content y. A squareness of the magnetic hysteresis is not a feature commonly observed in IV–VI DMSs. It is a signature that the distribution of Mn ions in the semiconductor lattice is uniform resulting in a uniform domain structure of the material below T_C. We did not observe elliptical magnetic hysteresis curves, a feature commonly present in GeTe-related DMSs [17].

The $M(B)$ curves at the lowest measured temperature, i.e, $T = 4.3$ K, were analyzed in order to determine the saturation magnetization value M_s. The M_s value was estimated according to the approach law proposed by Becker et al. [18], i.e.,

$$M(B) = M_s \left(1 - \frac{c}{B} - \frac{d}{B^2}\right) + \chi_{\mathrm{dia}} B, \qquad (3)$$

where c and d are fitting parameters, and the term $\chi_{\mathrm{dia}}B$ is related to the diamagnetic host lattice. The estimated M_s values are presented in Table I. The M_s values are an increasing function of the Mn content. The M_s values can be used to calculate another effective Mn content y_θ using the following equation

$$y_m = \frac{m_u M_s}{g J \mu_B N_A}, \qquad (4)$$

where m_u is the particle mass of the $Sn_{1-x-y}Si_xMn_yTe$ crystals and N_A is the Avogadro constant. The estimated y_m values are gathered in Table I. As we can clearly see for all our samples we have $y_\theta < y_m < y$ relation. We again confirm that the Mn content determined via the EDXRF method is higher than the Mn-contents obtained via magnetometric methods. That, in turn, is due to the presence of a large fraction of Mn ions coupled in pairs, triples, or more complex clusters or a fraction of Mn ions having lower total magnetic momentum than $J = S = 5/2$.

For the purposes of the estimation of the RKKY interaction exchange strength, we made calculations of the Curie temperature as a function of the Mn content y for different J_{pd} values (i.e., for different Mn-ion conducting hole exchange coupling constant). The calculations are based on the model proposed by Sherrington and Southern, described in detail in [19]. The calculations were done with the exponential damping factor $\lambda = 10$ nm and lattice parameter $a = 6.318$ Å. Results of these calculations are shown in Fig. 3.

As we can clearly see the obtained results point towards the conclusion that the J_{pd} exchange parameter for our samples ranges between 0.25 and 0.3 eV. This value is higher than that of $Sn_{1-x}Mn_xTe$ equal to 0.1 eV. Deviations from theoretical lines are due to the fact that the calculations were made for $n = 8 \times 10^{20}$ cm^{-3}, while n for our samples changes between $6–9 \times 10^{20}$ cm^{-3}. Also, the Si content in the samples varies slightly. We believe that an increase in the J_{pd} value for our samples is due to the silicon alloying.

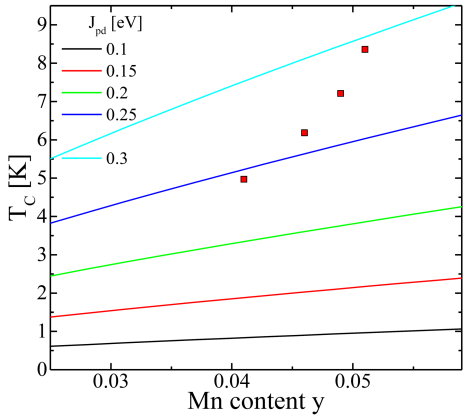

Fig. 3. The Curie temperature as a function of the Mn content y obtained experimentally (points) and calculated (lines) for different J_{pd} values.

7. Conclusions

We performed a series of structural, electrical, and magnetometric measurements characterizing different properties of $Sn_{1-x-y}Si_xMn_yTe$ crystals with different chemical contents, namely x and y. We observed two types of transitions via magnetic susceptibility measurements: (i) paramagnet–ferromagnet transition at $T < 10$ K due to carrier mediated RKKY magnetic interactions and (ii) an anomaly in the magnetic susceptibility related to the ferroelectric structural transition of the rhombohedral phase at $T \approx 75$ K. The presence of a well-defined magnetic hysteresis with square shape confirms that the ferromagnetic state present in our samples is related to homogeneous magnetic domain structure with narrow domain energy distribution. The contents of the magnetic ions determined via magnetometric methods are lower than the Mn contents determined via the EDXRF method indicating the presence of a large fraction of Mn ions being either short range coupled into small clusters like pairs, triples, or other entities or having lower total magnetic momentum than Mn in high-spin-state. The magnetic exchange constant of our samples is equal to 0.25–0.3 eV indicating an increase with respect to ternary $Sn_{1-x}Mn_xTe$.

Acknowledgments

The research was financed by the National Science Centre, Poland under project number 2018/30/E/ST3/00309.

References

[1] W. Dobrowolski, J. Kossut, T. Story, in: *Handbook of Magnetic Materials*, Ed. K.H.J. Buschow, Vol. 15, Elsevier, Amsterdam 2003, p. 289.

[2] J. Kossut, W. Dobrowolski, in: *Handbook of Magnetic Materials*, Ed. K.H.J. Buschow, Vol. 7, North-Holland, Amsterdam 1993, p. 231.

[3] S.A. Wolf, D.D. Awschalom, R.A. Buhrman, J.M. Daughton, S. von Molnar, M.L. Roukes, A.Y. Chtchelkanova, D.M. Treger, *Science* **294**, 1488 (2001).

[4] Y. Fukuma, H. Asada, M. Arifuku, T. Koyanagi, *Appl. Phys. Lett.* **80**, 1013 (2002).

[5] J. Cohen, A. Globa, P. Mollard, H. Rodot, M. Rodot, *J. Phys. (Paris)* **29**, C4-142 (1968).

[6] S. Eltink, H. Swagten, N. Stoffels, W. de Jonge, *J. Magn. Magn. Mater.* **83**, 483 (1990).

[7] P. Łazarczyk, T. Story, R.R. Gałązka, W. Mac, M. Herbich, A. Stachow-Wójcik, *J. Magn. Magn. Mater.* **176**, 233 (1997).

[8] A. Nadolny, J. Sadowski, B. Taliashvili et al., *J. Magn. Magn. Mater.* **248**, 134 (2002).

[9] B. Brodowska, W. Dobrowolski, M. Arciszewska, E.I. Slynko, V.K. Dugaev, *J. Alloys Comp.* **423**, 205 (2006).

[10] P.J.T. Eggenkamp, C.W.H.M. Vennix, T. Story, H.J.M. Swagten, C.H.W. Swüste, W.J.M. de Jonge, *J. Appl. Phys.* **75**, 5728 (1994).

[11] *State Diagrams of Binary Metal Systems: Reference Book*, Ed. N.P. Lyakishev, Mashinostroeniye, Moscow, three-volume edition, Vol. 1, 1996, p. 991; Vol. 2, 1997,p. 1023; Vol. 3, 2001, p. 872 (in Russian).

[12] P.B. Pereira, I. Sergueev, S. Gorsse, J. Dadda, E. Muller, R.P. Hermann, *Phys. Status Solidi B* **250**, 1300 (2013).

[13] R.F. Brebrick, *J. Phys. Chem. Solids* **24**, 27 (1963).

[14] L. Kilanski, M. Arciszewska, W. Dobrowolski, V. Domukhovski, V.E. Slynko, E.I. Slynko, *J. Appl. Phys.* **105**, 103901 (2009).

[15] R.E. Behringer, *J. Chem. Phys.* **29**, 537 (1958).

[16] P.B. Littlewood, *J. Phys. C* **13**, 4875 (1980).

[17] L. Kilanski, R. Szymczak, W. Dobrowolski, K. Szałowski, V.E. Slynko, E.I. Slynko, *Phys. Rev. B* **82**, 094427 (2010).

[18] R. Becker, W. Döring, *Ferromagnetismus*, Springer, Berlin 1939, p. 171 (in German).

[19] D. Sherrington, B.W. Southern, *J. Phys. F* **5**, L49 (1975).